International Journal of Luminescence and applications
Vol5 (4) December, 2015, pages 423-431

Luminescence Properties of Orange – Red Emitting $Sr_2MgSi_2O_7:Eu^{3+}$ Phosphor prepared by Solid State Reaction Method

[a]Ishwar Prasad Sahu*, [a]D. P. Bisen, [a]Nameeta Brahme, [a]Raunak Kumar Tamrakar

[a]School of Studies in Physics & Astrophysics, Pt. Ravishankar Shukla University, Raipur (C.G.)
Pin Code - 492010, India
[b]Department of Applied Physics, Bhilai Institute of Technology Durg (C.G.)
Pin Code - 491001, India
Corresponding author Email Id: **ishwarprasad1986@gmail.com***

Abstract

Europium doped di-strontium magnesium di-silicate phosphor namely: $Sr_2MgSi_2O_7:Eu^{3+}$ was prepared by the traditional high temperature solid state reaction method. The crystal structure of sintered phosphor was an akermanite type structure which belongs to the tetragonal crystallography with space group $P\bar{4}2_1m$. Energy dispersive X-ray spectroscopy (EDS) spectrum confirmed the elements present in $Sr_2MgSi_2O_7:Eu^{3+}$ phosphor. The thremoluminescence (TL) kinetic parameters such as activation energy (E), order of kinetics (b), and the frequency factor (S) of synthesized phosphor has been calculated using peak shape method. Photoluminescence (PL) measurements showed that the phosphor exhibited emission peak with good intensity at 613 nm (red emission) corresponding to $^5D_0 \rightarrow {}^7F_2$ and weak $^5D_0 \rightarrow {}^7F_1$ (590 nm) orange emission. The excitation spectra monitored at 613 nm show broad band from 225 to 325 nm ascribed to O–Eu charge-transfer (CTB) transition and the other peaks in the range of 350–410 nm originated from f–f transitions of Eu^{3+} ions. The strongest band at 395 nm can be assigned to $^7F_0 \rightarrow {}^5L_6$ transition of Eu^{3+} ions due to the typical f–f transitions within Eu^{3+} of $4f^6$ configuration. CIE color chromaticity diagram and ML spectra confirmed that the prepared $Sr_2MgSi_2O_7:Eu^{3+}$ phosphor exhibits orange–red emission. The mechanoluminescence (ML) intensity of $Sr_2MgSi_2O_7:Eu^{3+}$ phosphor increases linearly with increasing impact velocity of the moving piston, which suggests that this phosphor can be used as sensor to detect the stress of an object. Thus, the present investigation indicates the piezo-electricity is responsible to produce ML in prepared $Sr_2MgSi_2O_7:Eu^{3+}$ phosphor.

Keywords: XRD;FTIR; Photoluminescence; CIE color cordinates.

Introduction

Light-emitting diodes (LEDs) have recently attracted attention as novel sources for illuminating light. LEDs have several advantages over fluorescent lights, including a longer operating life, better energy efficiency and a mercury-free composition [1. It is well known that white LEDs are mainly fabricated by combining blue LEDs with a yellow-emitting phosphor ($YAG:Ce^{3+}$). However, the white light obtained has a poor color rendering, because the yellow emission of $YAG:Ce^{3+}$ lacks any red and blue-green emissions [2–4]. Recently, one solution to this problem has been to fabricate a white LED with high color rendering by combining red, green and blue emitting tricolor phosphors with irradiation by a near UV LED. Therefore, the development of red and green phosphors that show high emission intensities is desired [5].

Melilites, which are generally formulated as $M_2T(1)T(2)_2O_7$ (where M and T(1) are usually the alkaline earths or transition metals [M = Sr, Ca, Ba; and T(1) = Mg, Zn], and T(2) is usually Al, Ga, Si or Ge), have been investigated widely as optical materials [6], due to their tetragonal and non-centrosymmetric crystal structure. Lanthanides or transition metals can be accepted easily as constituents or dopants by the melilites, allowing the synthesis of high-quality doped single crystals [7]. The silicate matrix $Sr_2MgSi_2O_7$ is a typical melilite. Phosphors based on a silicates host is one of the most important luminescent materials and rare earth doped silicates usually have excellent thermal stability, high brightness, no radiation, long duration of afterglow and environmental stability. They have been studied widely with Eu^{2+} doping, which shows that a blue emission and long persistent luminescence by co-doping with some other rare earth ions [8]. Eu^{3+} ions were chosen as a luminescent species in many cases for the reasons of measurable lifetimes and simple luminescent spectra when compared to other rare earths [9]. It is interesting to investigate the luminescent properties of Eu^{3+} in $Sr_2MgSi_2O_7$ matrix with the purpose of synthesis of a low-cost and high efficiency red phosphor. Most of the silicate based phosphors which possess the tetragonal and non-centrosymmetric crystal structure, also have the ability to produce mechnoluminescence (ML) [10].

ML also known as Triboluminescence, is an important physical phenomenon where an emission of light is observed due to mechanical deformation of materials, when they are subjected to some mechanical stress like rubbing, cleavage, compressing, impulsive deformation, crushing, grinding, shaking etc. This phenomenon has been observed in many kinds of solids [11]. In the present studies, an impulsive deformation technique has been used. During the deformation of a solid, a great number of physical processes may occur within very short time intervals, which

may excite or stimulate the process of photon emission [12]. When a moving piston is applied to the phosphor, initially the ML intensity increases with time, attains a peak value and then decreases with time. Such a curve is known as the ML glow curve [13].

ML has found various important applications such as impact sensors in spacecrafts (the emission intensity can be used to determine the kinetic energy of impact), fracture sensor, damage sensor, stress sensor etc [14]. Until now, some phosphors with high ML, such as (red phosphor) $BaTiO_3$–$CaTiO_3$:Pr, (green phosphor) $SrAl_2O_4$:Eu, (yellow phosphor) ZnS:Mn, and (blue phosphor) $CaYAl_3O_7$:Eu etc., have been developed. At the same time, the high stabilities, such as resistance of water, thermal stability are also important for the application of ML. More ML phosphors with strong ML intensity and high stability are needed [15, 16].

In this paper, we report the synthesis of Europium doped di-strontium magnesium di-silicate phosphor namely: $Sr_2MgSi_2O_7:Eu^{3+}$ phosphor by high temperature solid state reaction method. This paper reports the structural characterization of the phosphor on the basis of XRD and EDX analysis. Luminescence studies were also carried out using thermoluminescence (TL), photoluminescence (PL), mechanoluminescence (ML) techniques.

Experimental
Material Preparation

Europium doped di-strontium magnesium di-silicate namely $Sr_2MgSi_2O_7:Eu^{3+}$ phosphor was prepared by the high temperature solid state reaction method. The raw materials are strontium carbonate [$SrCO_3$ (99.90%)], magnesium oxide [MgO (99.90%)], silicon di-oxide [SiO_2 (99.99%)] and europium oxide [Eu_2O_3 (99.99%)], all of analytical grade (A.R.), were employed in this experiment. Boric acid (H_3BO_3) was added as flux. Initially, the raw materials were weighed according to the nominal compositions of $Sr_2MgSi_2O_7:Eu^{3+}$ phosphor. Then the powders were mixed and milled thoroughly for 2 hour using mortar and pestle. The grinded sample was placed in an alumina crucible and subsequently fired at 1200°C for 3 hours. The chemical reaction used for stoichiometric calculation is:

$$4SrCO_3 + 2MgO + 4SiO_2 + 2Eu_2O_3 \Longrightarrow 2Sr_2MgSi_2O_7:Eu^{3+} + 4CO_2 + 3O_2 \uparrow$$

At last the nominal compounds were obtained after the cooling down of programmable furnace and products were finally ground into powder for characterizing the phosphors. Solid state reaction method is widely used to prepare silicate based phosphors because samples prepared using this method has good luminescence and very good morphology [17].

Structural and Luminescence Characterization Technique

The crystal structure of the prepared $Sr_2MgSi_2O_7:Eu^{3+}$ phosphor was characterized by powder XRD analysis. Powder XRD pattern has been obtained from Bruker D8 advanced X-ray powder diffractometer and the data were collected over the 2θ range 20°-70°. The X-rays were produced using a sealed tube (CuKα) radiation source and the wavelength of X-ray was (1.54060 Å). The X-rays were detected using a fast counting detector based on Silicon strip technology (Bruker LynxEye detector). The crystal structure of the prepared sample was verified with the help of Joint Committee of Powder Diffraction Standard Data (JCPDS) file. (JCPDS: 75-1736). Energy dispersive X-ray spectroscopy (EDS) was used for the elemental analysis of the prepared phosphor. The TL glow curves were recorded with the help of TLD reader 1009I by Nucleonix (Hyderabad, India Pvt. Ltd.). The excitation and emission spectra were recorded on a Shimadzu (RF 5301-PC) spectrofluorophotometer using the Xenon lamp (365 nm) as excitation source when measuring. The color chromaticity coordinates were obtained according to Commission International de I'Eclairage (CIE) 1931. The ML measurement was observed by the home made lab system comprising of RCA-931A photomultiplier tube (PMT). The ML glow curve can be plotted with the help of SM-340 application software installed in a computer attached with the storage oscilloscope. The ML spectrum was recorded with the help of different band pass interference (400–700 nm) filters. All measurements were carried out at the room temperature.

Experimental setup for Mechanoluminescence (ML) measurement

The experimental set up used for the impulsive deformation of ML was shown in Fig.1. A load (moving piston) of particular mass and shape was dropped from different heights [different impact velocities (υ_0)] for striking the prepared $Sr_2MgSi_2O_7:Eu^{3+}$ phosphor. In this experiment, the mass of the dropping load was 400 g and shape of the load was cylindrical. The phosphor under study was placed on the upper surface of a transparent lucite plate and it was then covered with a thin aluminum foil and fixed with an adhesive tape. The foil reflects light and prevents scattering of the fragments during the impact of a moving piston onto the prepared phosphor. This arrangement eliminates the error in the ML measurement due to the scattering of the crystallite fragments during the impact of the load onto the phosphor. The housing is made up of thick soft iron to provide shielding from light and magnetic field. The slit arrangement at the window is provided to adjust the size of

the window according to the incident beam. When the phosphor placed on the lucite plate was crushed by impact of the moving piston, light is emitted [18].

By changing the distance between the moving piston to be dropped and the sample placed on the lucite plate, the impact velocity of the load, could be changed from 198 cm/s to 313 cm/s (20 to 50 cm height). Since the pulley and the guiding cylinder used were of negligible friction, the impact velocity of moving piston was taken as [$\upsilon_0 = \sqrt{2gh}$ (where "**g**" is the acceleration due to gravity and "**h**" is the height through which the load is dropped freely)]. An RCA 931A photomultiplier tube (PMT) was placed below the transparent lucite plate. The PMT was run at 750 Volts. The output of PMT was connected to the phosphorescent screen oscilloscope (Scientific 300 MHz, SM 340). The ML glow curve can be plotted with the help of SM-340 application software installed in a computer attached with the storage oscilloscope [19].

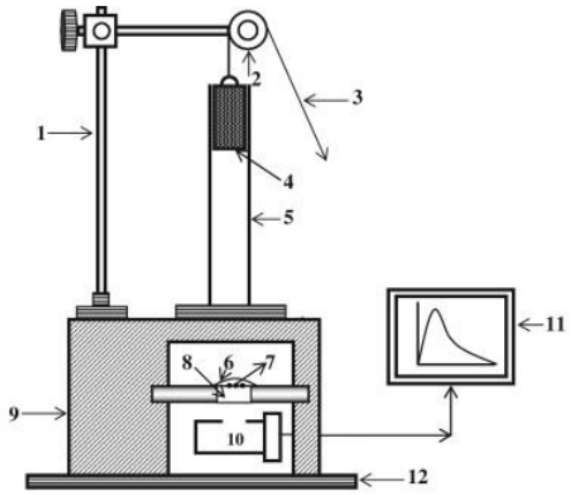

Fig. 1 Schematic diagram of the experimental setup for ML measurement

In the Fig. 1, **1** - Stand; **2** - Pulley; **3** - Metallic wire; **4** - Load; **5** - Guiding cylinder; **6** - Aluminium foil; **7** - Phosphor; **8** - Transparent Lucite plate; **9** - Wooden block; **10** - Photomultiplier tube (PMT); **11** - Storage oscilloscope; **12** - Iron base mounted on a table.

Results and Discussions

XRD Analysis

The typical XRD patterns of $Sr_2MgSi_2O_7:Eu^{3+}$ with that of the standard JCPDS file are shown in Fig. 2. Nearly, all the diffraction peaks of the resultant phosphor are consistent with Joint Committee Powder Diffraction Standard data (JCPDS) file (JCPDS: 75-1736) [20]. The position and intensity of diffraction peaks of $Sr_2MgSi_2O_7:Eu^{3+}$ are well matched with the standard JCPDS file. The crystal structure of the $Sr_2MgSi_2O_7:Eu^{3+}$ phosphor was an akermanite type structure which belongs to the tetragonal crystallography with space group $P\bar{4}2_1m$, this structure is a member of the melilite group and forms a layered compound. The small amount of impurity did not change the crystal ctructure of the sintered phosphor. The radius of Eu^{2+} (1.12 Å) is very close to that of Sr^{2+} (about 1.12 Å) rather than Mg^{2+} (0.65 Å) and Si^{4+} (0.41 Å). Therefore, the Dy^{3+} ions are expected to occupy the Sr^{2+} sites in the $Sr_2MgSi_2O_7:Eu^{3+}$ phosphor.

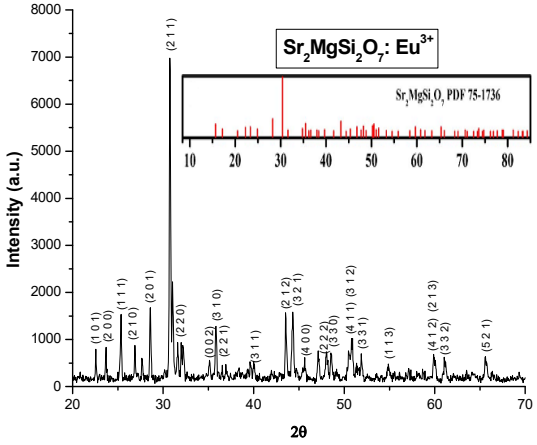

Fig. 2 XRD pattern of $Sr_2MgSi_2O_7:Eu^{3+}$ phosphor

Energy dispersive X-ray spectroscopy (EDS)

Fig. 3 shows the an Energy dispersive x-ray spectroscopy (EDS) spectra of $Sr_2MgSi_2O_7:Eu^{3+}$ phosphor. The composition of the powder sample has been measured using EDS. There was no other emission apart from strontium (Sr), magnesium (Mg) silicon (Si), oxygen (O) and europium (Eu) in EDS spectra of the sample. In the spectrum, intense peaks are present which confirm the formation of $Sr_2MgSi_2O_7:Eu^{3+}$ phosphor (Table 1).

Table 1 Composite element of $Sr_2MgSi_2O_7:Eu^{3+}$ phosphor

Sr. N.	Standard	Elements	Weight %	Atomic %
1	SiO_2	O K	33.85	63.59
2	MgO	Mg K	4.34	5.29
3	SiO_2	Si K	13.53	14.50
4	SrF_2	Sr L	47.04	16.19
5	EuF_3	Eu L	1.23	0.42
Total			**99.99**	**99.99**

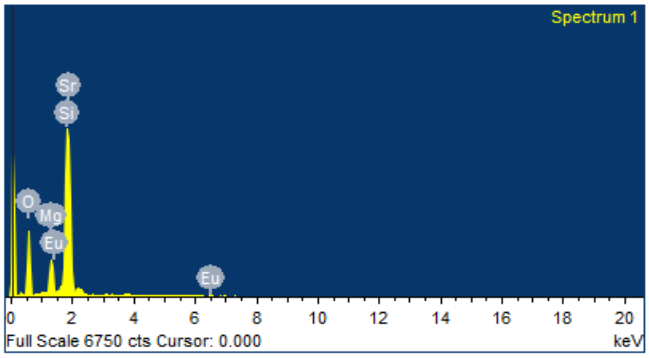

Fig. 3 EDS spectra of $Sr_2MgSi_2O_7:Eu^{3+}$ phosphor

Thermoluminescence (TL)

Thermoluminescence (TL) is thermally stimulated emission of light from an insulator or semiconductor, following the previous absorbtion of energy from ionizing radiations. On subsequent heating the energy may be released and some of it may be in the form of light [21, 22]. TL measurements provide information on the nature of the traps in the long persistent phosphors [23]. The TL glow curves **of** $Sr_2MgSi_2O_7:Eu^{3+}$ were measured (Fig. 4). The phosphors were first irradiated for 10 min. using 365 nm UV source, the irradiated samples were heated at a linear heating rate of 5°C/s, from room temperatures to 300°C. A single glow peak as obtained at 172.41°C, indicating that the electron traps involved are deep enough and high energy is required to release the trapped electrons; hence long storage of trapped charge carriers at normal working temperature is achieved and thus the thermal stability is ensured. The single isolated peak due to the formation of only one type of luminescence center which is created due to the UV irradiation. The recombination center associated with the glow at the temperature interval arises from the presence of liberated pairs, which are probably the results from the thermal release of electron/holes from electron/hole trap level and recombine at the color centers. The TL kinetic parameters are calculated and listed in Table 2.

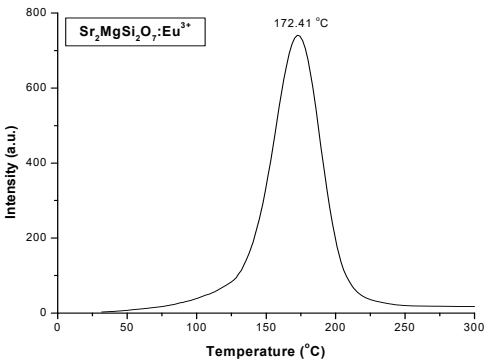

Fig. 4 TL glow curve of $Sr_2MgSi_2O_7:Eu^{3+}$ phosphor for 10 min UV irradiation

Determination of kinetic parameters

The TL emission characteristic of a phosphor material mainly depends on the kinetic parameters describing the trapping-emitting
centers.There are various methods for evaluating the trappi ng para-meters from TL glow curves [24]. For example, when one of the TL glow peaks is highly isolated from the others, experimental method such as peak shape method is suitable to determine kinetic parameters. The TL parameters for the prominent glow peak of prepared phosphor were calculated using the peak shape method [25]. Fig. 5 shows the schematic diagram of glow curve peak shape method.

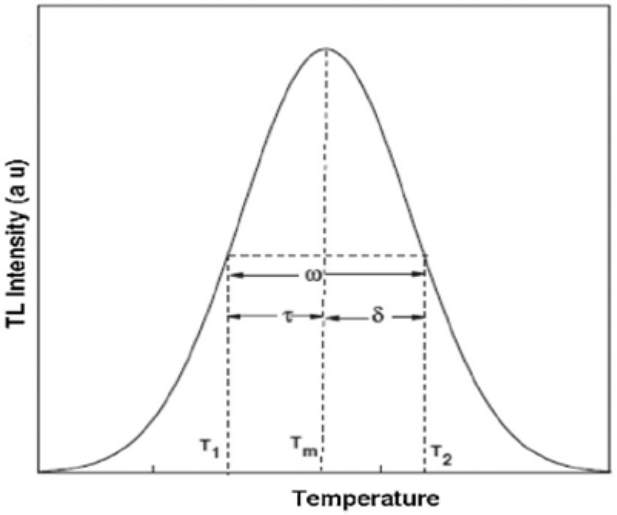

Fig. 5 Schematic diagram of glow curve peak shape method

Glow curve peak shape method: Using the glow curve peak shape method the different shape parameters of the present $Sr_2MgSi_2O_7:Eu^{3+}$ phosphor namely the total half intensity $\omega = T_2 - T_1$ ($\tau+\delta$), τ is the half width at the low temperature side of the peak or the low temperature half width ($\tau = T_m-T_1$); δ is the half width towards the fall-off side of the glow peak or the high temperature half width ($\delta = T_2-T_m$), and T_m is the peak temperature and T_1 and T_2 are temperature on either side of T_m corresponding to half peak intensity were determined and presented in Table 2 [26].

Order of kinetics (*b*): The mechanism of recombination of de-trapped charge carriers with their counterparts is known as the order of kinetics (*b*). The order of kinetics can be predicted from shape of glow curve by using symmetry factor or geometric factor (μ_g) stated by Chen can be given as

$$\mu_g = \delta/\omega = T_2\text{-}T_m/T_2\text{-}T_1 \quad (1)$$

The symmetry factor is to differentiate between first and second order TL glow peak. (μ_g) = 0.39-0.42 for the first order kinetics; (μ_g) = 0.49-0.52 for the second order kinetics and (μ_g) = 0.43-0.48 for the mixed order of kinetics [27].

Activation energy (E): The knowledge about trapping parameters for calculating trap information in traps centre such as required energy for escaping one electron from trap centre known as activation energy or trap depth "E". So, the trap depth calculated by different methods proposed by several authors [28]. Trap depth for second order kinetics is calculated using the equation (2)

$$E = 2kT_m\left(1.76\frac{T_m}{\omega} - 1\right) \quad (2)$$

Where, k is Boltzmann constant, E is activation energy, T_m is temperature of peak position.

Frequency factor (s): Frequency factor reflects the probability to escape of electrons from the traps after exposure of ionizing radiation and it is one of the important parameter of the phosphor characterization. Once the order of kinetics and activation energy were determined, the frequency factor (s) can be calculated from the equation (3)

$$\frac{\beta E}{kT_m^2} = s\left[1 + (b-1)\frac{2kT_m}{E}\right]\exp(E/KT_m) \quad (3)$$

Where b is order of kinetics, and β is the heating rate. In the present work $\beta = 5^oCs^{-1}$.

The calculated kinetic parameters of $Sr_2MgSi_2O_7:Eu^{3+}$ phosphor by the peak shape method is given in Table 2. In our case, the value of shape factor (μ_g) is 0.48, which indicates that it is a case of non-first order kinetics, approaching towards second order, responsible for deeper trap depth [29].

Table 2 Activation Energy (E), Frequency Factor (s^{-1}) and Shape factor (μ_g) for UV irradiated $Sr_2MgSi_2O_7:Eu^{3+}$ phosphor

UV Min	HTR	T_1 (°C)	T_m (°C)	T_2 (°C)
10	5	151.45	172.41	191.8

τ	δ	ω	μ = δ/ω	Activation Energy	Frequency Factor
20.96	19.39	40.35	0.48	1.41	5.60×10^{15}

Photoluminescence (TL)

The emission spectrum of $Sr_2MgSi_2O_7:Eu^{3+}$ phosphor under 395 nm excitation was shown in Fig. 6. It can be seen that its emission spectra are all composed of several sharp lines from the characteristic Eu^{3+} emission. The excitation spectrum of $Sr_2MgSi_2O_7:Eu^{3+}$ phosphor exhibit a broad band in the UV region centered at about 269 nm, and several sharp lines between 300 to 400 nm. Eu^{3+} ions has a $4f^6$ configuration [30]. When Eu^{3+} is linked to the O ligand, there is a chance of electron transfer from O^{2-} to Eu^{3+} to form $Eu^{2+} - O^-$ (simply Eu–O). During this, there is a broad absorption band at 220– 300 nm, depending on the host. This is known as the Eu–O charge transfer band (CTB).

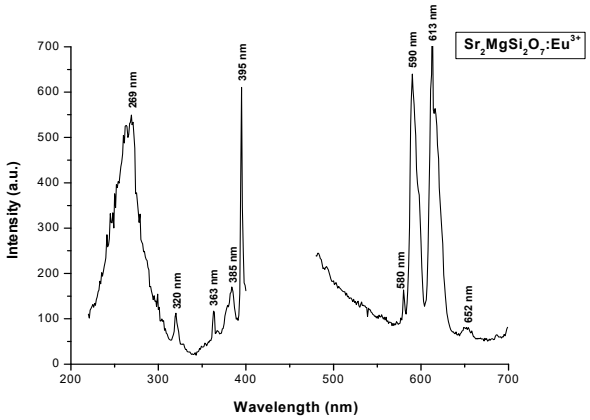

Fig. 6 Excitation and emission spectra of $Sr_2MgSi_2O_7:Eu^{3+}$ phosphor

It can be seen from Fig. 6, the excitation spectrum is composed of two major parts: (1) the broad band between 220 and 300 nm, called charge transfer state (CTS) band due to the europium-oxygen interactions, which is caused by an electron transfer from an oxygen 2p orbital to an empty 4f shell of europium and the strongest excitation peak at about 269 nm. (2) sharp peaks between 300 to 400 nm. The strongest sharp peak is located at 395 nm corresponding to $^7F_0 \rightarrow {}^5L_6$ transition of Eu^{3+}. Other weak excitation peaks are located at 320, 363 and 386 nm are related to the intra-configurational 4f–4f transitions of Eu^{3+} ions in the host lattices [31]. The prepared $Sr_2MgSi_2O_7:Eu^{3+}$ phosphor can be excited by near UV (NUV) at about 395 nm effectively and hence can match well with UV -LED, showing a potential for practical applications.

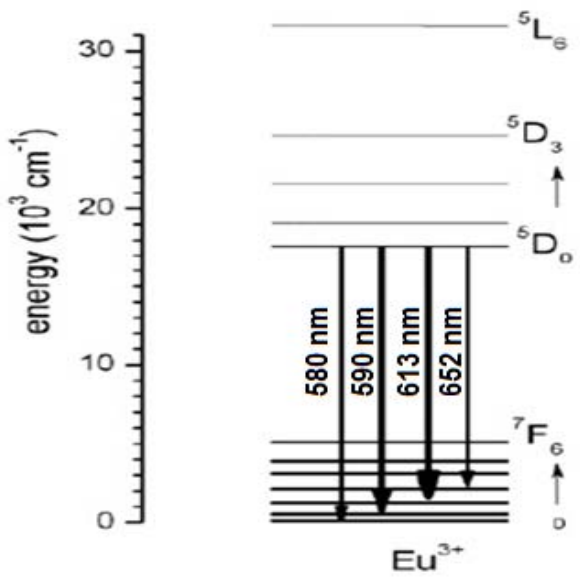

Fig. 7 Schematic energy level diagram of $Sr_2MgSi_2O_7:Eu^{3+}$ phosphor

The emission spectra of $Sr_2MgSi_2O_7:Eu^{3+}$ phosphor is shown in Fig. 6 in the range of 400 to 700 nm. Under the 395 nm excitation, the emission spectrum is composed of a series of sharp emission lines, corresponding to transitions from the excited states $^5D_0$ to the ground state $^7F_{j\ (j\ =\ 0,1,2,3)}$ [32]. The orange emission at about 590 nm belongs to the magnetic dipole $^5D_0 \rightarrow {}^7F_1$ transition of Eu^{3+}, and the transition hardly varies with the crystal field strength. The red emission at 613 nm ascribes to the electric dipole $^5D_0 \rightarrow {}^7F_2$ transition of Eu^{3+} ions, which is very sensitive to the local environment around the Eu^{3+}, and depends on the symmetry of the crystal field. It is found that the 590 and 613 nm emissions are the two strong peaks. [33]. One site, Sr (I), is inversion symmetry and the other site, Sr (II), is non-inversion symmetry. When doped in $Sr_2MgSi_2O_7:Eu^{3+}$ ions occupy the two different sites of Sr (I) and Sr (II). Other two emission peaks located at 580 and 652 nm are relatively weak, corresponding to the $^5D_0 \rightarrow {}^7F_0$ and $^5D_0 \rightarrow {}^7F_3$ typical transitions of Eu^{3+} ions respectively. The strongest emission is associated to the Eu^{3+} electric-dipole transition of $^5D_0$-$^7F_1$, and which implies that the Eu^{3+} occupies a center with asymmetry in the host lattice. For $Sr_2MgSi_2O_7:Eu^{3+}$ prepared in our experiment, the strongest red emission peak is located at 613 nm [34]. Fig. 7 shows the schematic energy level diagram of Eu^{3+} ions in the $Sr_2MgSi_2O_7$ host depicting different emissions bands.

CIE Chromaticity Coordinate

The luminescence color of the samples excited under 395 nm has been characterized by the CIE (Commission International de I'Eclairage) 1931 chromaticity diagram [35]. The emission spectrum of the $Sr_2MgSi_2O_7:Eu^{3+}$ phosphor was converted to the CIE 1931 chromaticity using the photoluminescent data and the interactive CIE software (CIE coordinate calculator) diagram as shown in Fig. 8.

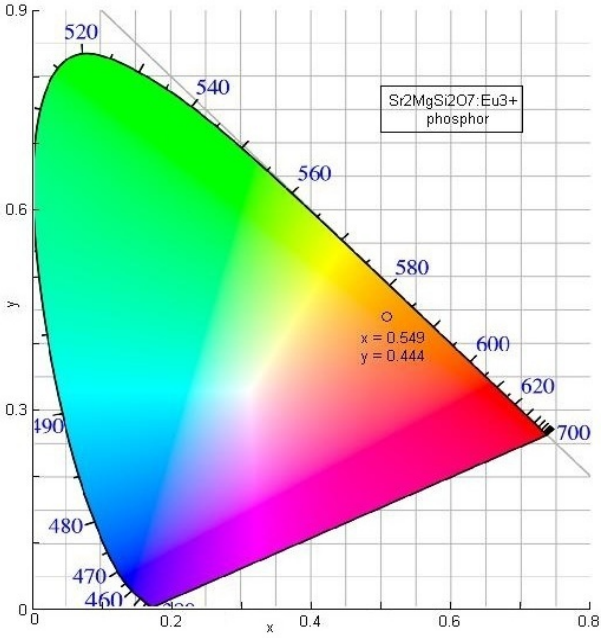

Fig. 8 CIE chromaticity diagram of $Sr_2MgSi_2O_7:Eu^{3+}$ phosphor

Luminescence colors of Eu^{3+} doped $Sr_2MgSi_2O_7$ phosphor are placed in the orange-red (x = 0.549, y = 0.444), corners. The chromatic co-ordinates of the luminescence of this phosphor are measured and reached to orange-red luminescence.

Mechanoluminescence (ML)

Fig. 9 shows that the characteristics curve between ML intensity versus time for different heights (h = 20, 30, 40, 50 cm). The phosphor was fracture via dropping a load [moving piston] of particular mass (400 g) and cylindrical shape on the $Sr_2MgSi_2O_7:Eu^{3+}$ phosphor. The velocity of the moving piston, holding the impact mass, could be changed, by changing the height through which it was dropped. Every time for the ML measurement, the quantity of $Sr_2MgSi_2O_7:Eu^{3+}$ phosphor was kept constant (8 mg). When the moving piston is dropped onto the prepared phosphor at different height, light is emitted. The photon emission time is nearly 2 ms, when prepared $Sr_2MgSi_2O_7:Eu^{3+}$ phosphor fractures. In these ML measurements, maximum ML intensity has been obtained for the 50 cm dropping height and ML intensity increases linearly with the increases the falling height of the moving piston. The sintered $Sr_2MgSi_2O_7:Eu^{3+}$ phosphor was not irradiated by any excitation source [36].

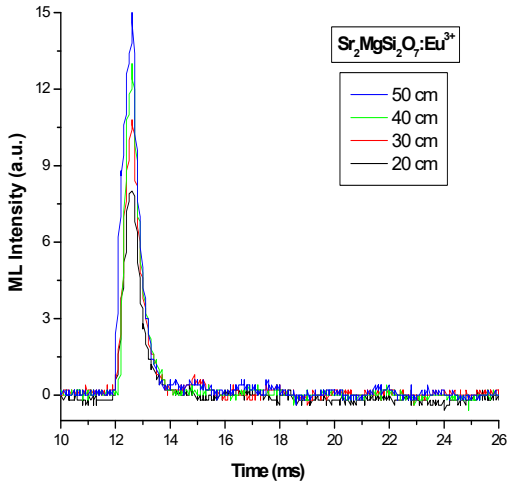

Fig. 9 ML intensity versus time curve of $Sr_2MgSi_2O_7:Eu^{3+}$ phosphor

Fig. 10 shows the characteristics curve of ML intensity versus impact velocities for $Sr_2MgSi_2O_7:Eu^{3+}$ phosphor. It is seen that, ML intensity increases linearly with increasing impact velocity [$\sqrt{2gh}$, (where "**g**" is the acceleration due to gravity and "**h**" is the height through which the load is dropped freely)] of the moving piston. The ML intensity of $Sr_2MgSi_2O_7:Eu^{3+}$ phosphor increases linearly with increasing the mechanical stress [37].

When the load or piston makes an impact on the crystal with an initial velocity v_0, the former decelerates and after a particular time its velocity becomes zero. The time dependence of the velocity of the piston may be written as

$$v = v_0 \exp(-\beta v_o t) \quad (4)$$

Where β is a constant, equation (4) can be written as

$$\frac{dx}{dt} = v_0 \exp(-\beta v_o t) \quad (5)$$

Where dx is the compression of the crystal during the time interval dt.
Integrating equation (5), we have

$$x = \frac{1}{\beta}\exp(-\beta v_o t) + C \quad (6)$$

x = 0 for t = 0, therefore, equation (6) may be written as

$$x = \frac{1}{\beta}[1 - \exp(-\beta v_o t)] \quad (7)$$

The prepared phosphor is in powder form and the impact velocities compress it to a certain extent, but this does not change significantly with increasing impact velocity. Equation (7) shows that impact time remains mostly unchanged with increasing impact velocity because there is no significant change in compression, which is expressed by 'x' in equation (9). This may be one possible reason why the time that corresponds to the peak ML intensity does not change significantly with increasing impact velocity.

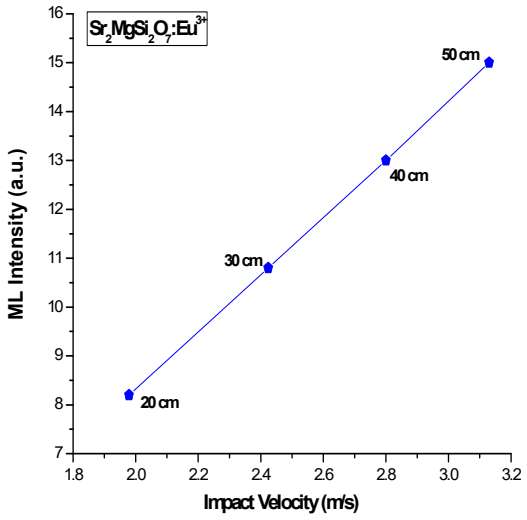

Fig. 10 ML intensity versus impact velocity curve of $Sr_2MgSi_2O_7:Eu^{3+}$ phosphor

Fig. 11 shows the realtion between the time corresponds to ML signal peak and impact velocity of $Sr_2MgSi_2O_7:Eu^{3+}$ phosphor. It can be seen that time for peak ML intensity does not change significantly with increasing impact velocity [38].

The relationship between semi-log plot of ML intensity versus $(t–t_m)$ for $Sr_2MgSi_2O_7:Eu^{3+}$ phosphor is shown in Fig. 12, and the lines were fitted using the following equation with Origin Pro 8.0

$$\tau = \frac{1}{slop \quad of \quad straight \quad line} \quad (8)$$

Curve fitting results show that decay constant (τ) varies from 0.80 to 0.84 ms (Table 3).

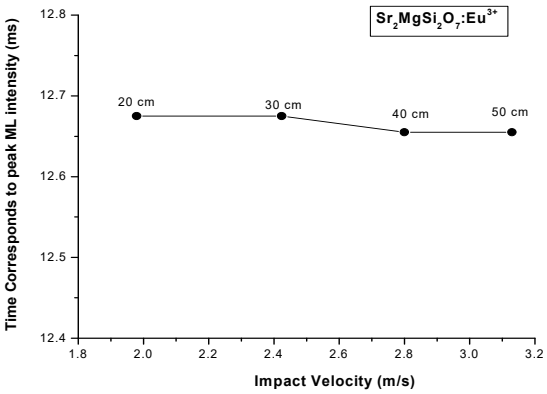

Fig. 11 Time corresponds to ML signal peak with impact velocity of $Sr_2MgSi_2O_7:Eu^{3+}$ phosphor

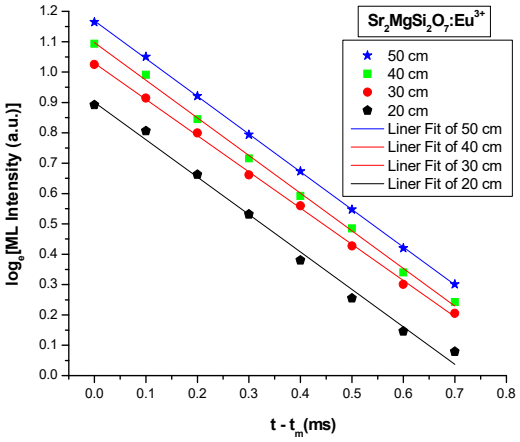

Fig. 12 Semi-log plot of ML intensity versus $(t - t_m)$ for $Sr_2MgSi_2O_7:Eu^{3+}$ phosphor

Table 3 Calculation of ML decay constant

Impact velocity	20 cm	30 cm	40 cm	50 cm
τ Decay constant(ms)	0.81	0.84	0.82	0.80

Fig. 13 shows that the ML spectrum of $Sr_2MgSi_2O_7:Eu^{3+}$ phosphor. The peak location of the ML spectra (~ 600 nm) ornge - red emission, CIE choromaticity diagram (orange - red emission) and PL spectra suggests that the prepared $Sr_2MgSi_2O_7:Eu^{3+}$ phosphor emit orange – red color.

When a mechanical stress, such as compress, friction, and striking, was applied on the sintered $Sr_2MgSi_2O_7:Eu^{3+}$ phosphors, piezo-electric field can be produced. During the impact on the material, one of its newly created surfaces gets positively charged and the other surface of the crack gets negatively charged. Thus, an intense electric field of the order of 10^6 - 10^7 Volt cm^{-1} is produced [see Fig.14].

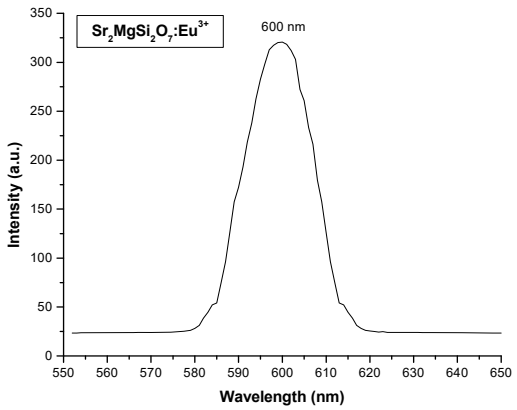

Fig. 13 ML spectra of $Sr_2MgSi_2O_7:Eu^{3+}$ phosphor

Under such order of electric field, the ejected electrons from the negatively charged surface may be accelerated and their impact on the positively charged surfaces may excite the luminescence center such as Eu^{3+} [39]. Subsequently, the de-excitation of excited Eu^{3+} ions may give rise to the light emission. With the increasing impact velocity, more compression of the sample takes place, and therefore, more area of the newly created surface takes place. Thus, the ML intensity will increase with increasing value of the impact velocity. The stress near the tip of a moving crack is of the order of $Y/100 \approx 10^{10}$ dynes/cm^2 = 10^9 Newton/m^2 (where Y is the Young's modulus of the materials). Thus, a fixed charge density will be produced on the newly created surfaces and the increase in the ML intensity will primarily be caused by the increase in the rate of newly created surface area with increasing impact velocity. Moreover, the total ML intensity will also increase with impact velocity, because more compression of the sample will create more surfaces with increasing impact velocity [40].

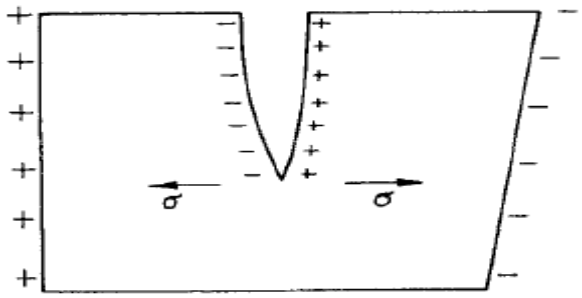

Fig. 14 Langevin model for the piezo-electrification induce phosphor

From Fig. 10, it can be seen that with increasing impact velocity, ML intensity also increases linearly;this suggests that the phosphor can be used as sensor to detect the stress of an object [41].

CONCLUSION

A orange–red emitting $Sr_2MgSi_2O_7:Eu^{3+}$ phosphor was synthesized by high temperature solid state reaction method at 1200°C and its structural characterization and luminescence properties were investigated. The structure of prepared phosphor was confirmed by XRD.. PL measurements showed that the phosphor exhibited emission peak with good intensity at 590 and 613 nm, corresponding to $^5D_0 \rightarrow {}^7F_1$ orange emission and weak $^5D_0 \rightarrow {}^7F_2$ red emission. CIE color chromaticity diagram and ML spectra confirmed that the phosphor exhibits orange–red emission. It is worthy to note that the dependence between ML intensity of $Sr_2MgSi_2O_7:Eu^{3+}$ and the impact velocity of the moving piston is close to linearity, which suggests this phosphor can also be used as sensor to detect the stress of an object.

References:

1. H. Y. Jiao, Y. Wang, Physica B 2012; 407: 2729-2733
2. R. Yu, Y. Guo, L. Wang, H. M. Noh, B. K. Moon, B. C. Choi, J. H. Jeong, J. Lumin. 2014; 155:317-321.
3. H. Nagabhushana, D.V. Sunitha, S.C. Sharma, B. D. Prasad, B.M. Nagabhushana, R.P.S. Chakradhar, 2014; 595:192-199.
4. Z. Wang, S. Lou, P. Li, J. Lumin. 2014; 156: 87-90.
5. Y. Kojima, M. Numazawa, T. Umegaki, J. Lumin. 2012; 132:2648-2652.
6. H. Liu, Y. Hao, H. Wang, J. Zhao, P. Huang, B. Xu, J. Lumin. 2011; 131:2422-2426.
7. I. P. Sahu, D. P. Bisen, Raunak Kumar Tamrakar, Ravi Shrivastava, Res. Chem. Intermed. (2015), DOI 10.1007/s11164-015-2120-4.
8. W. Pan, G. Ning, X. Zhang, J. Wang, Y. Lin, J. Ye, J. Lumin. 2008; 128: 1975-1979.
9. G.J. Talwar, C.P. Joshi, S.V. Moharil, S.M. Dhopte, P.L. Muthal, V.K. Kondawar, J. Lumin. 2009; 129: 1239-1241.
10. I. P. Sahu, J Mater Sci: Mater Electron, (2015), DOI 10.1007/s10854-015-3327-2.
11. D.R. Vij, Luminescence of Solids, Plenum Press, New York (1998).
12. C. N. Xu, T. Wantanabe, M. Akiyama, and X. G. Zheng, Appl. Phys. Lett. 1999; 74: 1236 – 1238.
13. I. P. Sahu, D. P. Bisen, N. Brhame, R.K. Tamrakar, R. Shrivastava J Mater Sci: Mater Electron, (2015), DOI 10.1007/s10854-015-3563-5.
14. C. N. Xu, T. Wantanabe, M. Akiyama, and X. G. Zheng, Appl. Phys. Lett. 1999; 74: 2414-2416.
15. C. N. Xu, X. G. Zheng, M. Akiyama, K. Nonaka, and T. Watanabe, Appl. Phys. Lett. 2000; 76: 179 – 181
16. C. N. Xu, X. G. Zheng, T. Wantanabe, M. Akiyama, I. Usui, Thin Solid Films 1999; 352: 273 -278.
17. I P. Sahu, D. P. Bisen, N. Brahme, M. Ganjir, Lumin. J. Biol. Chem. Lumin. 2015; DOI 10.1002/bio.2900
18. I. P. Sahu, D. P. Bisen, N. Brahme, L. Wanjari, R. K. Tamrakar, Res. Chem. Intermed. (2015) DOI:10.1007/s11164-015-1929-1.
19. I. P. Sahu, D. P. Bisen, N. Brahme, R. Sharma, Res. Chem. Intermed. (2014) DOI 10.1007/s11164-014-1767-6.
20. JCPDS file number 75 - 1736, JCPDS International Center for Diffraction Data.
21. S. Basuna, G.F. Imbuschb, D.D. Jiac, W.M. Yenc, J. Lumin. 104 (2003) 283.
22. R. Chen, Y. Kirsh, Pergamon Press (1981) 167.
23. R. Chen, S.W.S. McKeever, World Scientific (1997).
24. I. P. Sahu, P. Chandrakar, R. N. Baghel, D. P. Bisen, N. Brahme, R.K. Tamrakar, J. alloys. comp. 2015; 649: 1329-1338.
25. C. Y. Li, Q. Su, J. R. Qiu, J. Lumin. 24 (2003) 19.
26. H. N. Luitel, T. Watari, R. Chand, T. Torikai, M. Yada, J. Mater. 2013 (2013) 10.
27. I. P. Sahu, D. P. Bisen, N. Brahme, Displays, 2014; 35: 279 – 286.
28. T. Katsumata, R. Sakai, S. Komuro, T. Morikawa, J. Electrochem. Soc. 150 (2003) H111.
29. Z. Yuan, C. Chang, D. Mao, W. Ying, J. Alloys Compd. 377(1–2), (2004) 268–271.
30. S. P. Kuang, K. Liang, J. Liu, Y. M. Mei, M. Jiang, Z. C. Wu, D. X. Li, Optik. 2014; http://dx.doi.org/10.1016/j.ijleo.2013.12.037.
31. J. Liu, K. Liang, Z. C. Wu, Y. M. Mei, S. P. Kuang , D. X. Li, Ceramics International, 2014; 40: 8827–8831.
32. X. Zhang, A. Marathe, S. Sohal, M. Holtz, M. Davis, Louisa J. H. Weeks, J. Chaudhuri, J. Mater. Chem., 2012; 22: 6485.
33. M. Xu, L. Wang, L. Liu, D. Jia, R. Sheng, J. Lumin., 2014; 146: 475–479.
34. I. P. Sahu, D. P. Bisen, N. Brahme, R. K. Tamrakar, J. Radiat. Res. Appl. Sci. 2015; 8: 104–109.
35. I. P. Sahu, D. P. Bisen, N. Brahme, J. Radiat. Res. Appl. Sci. 2015; (8)3: 381-388.
36. CIE, International Commission on Illumination, Publication CIE no. 15, (E-1.3.1), 1931
37. I. P. Sahu, D. P. Bisen, N. Brahme, Displays 2015; 38: 68 - 76.
38. I. P. Sahu, D. P. Bisen, N. Brahme, Lumin. J. Biol. Chem. Lumin. 2015; 30 (5): 526-532.
39. Zhang H, Yamada H, Terasaki N, Xu C N, Int. J. Mod Phys B, 2009; 23 (6-7): 1028 – 1033.
40. H. Zhang, H. Yamada, N. Terasaki, C.N. Xu, Thin Solid Films 518 610 – 613 (2009).
41. I. P. Sahu, D. P. Bisen, N. Brahme, R. K. Tamrakar, J. Lumin, 2015; 167: 278-288.